2012

Preparation and characterization of a self-crimp side-by-side bicomponent electrospun material

Yang Han
Virginia Commonwealth University

PREPARATION AND CHARACTERIZATION OF A SELF-CRIMP SIDE-BY-SIDE BICOMPONENT ELECTROSPUN MATERIAL

A thesis submitted in partial fulfillment of the requirements for the degree of Master of Science in Biomedical Engineering at Virginia Commonwealth University.

by

YANG HAN

B.S., Donghua University, 2010

Director: GARY L. BOWLIN, PH.D,

PROFESSER, VIRGINIA COMMONWEALTH UNIVERSITY

Virginia Commonwealth University

Richmond, Virginia

August, 2012

Acknowledgement

It has been very fortunate for me to be able to come to grad school and work in my most interested field in biomedical engineering: tissue engineering. All these realized with the great help from Dr. Bowlin. Thank you Dr. Bowlin. During the last two years he gave me lots of support and insightful opinions on my research. There was one conversation between us that I would always remember. Several months after working on this side-by-side bicomponent material research, I got frustrated and doubt it would not work. I went to Dr. Bowlin and told him I wanted to change my research direction and also take some cell biology and biochemistry courses, because "I feel like I know nothing". Dr. Bowlin said, "This feeling of insufficiency will always be there when you do your research. No one can know all about everything." He told me to concentrate on what I have learnt and think about how to use them, rather than blindly running into different subjects. "Try to contribute on what you already specialized in and be who you really are, but no one else." He said. Thanks to this conversation I was able to restart this project and finally finished it as my thesis. Now I'm very proud of myself for proposing the initial design of this research and being able to finish it with encouraging results. If it's not Dr. Bowlin this wouldn't have happened.

I also want to thank Dr. Simpson and Dr. Yang for being my committee professors. Dr. Simpson gave great support for my research by borrowing me his scaffold stretchers and opening his lab to me. When I asked about the stretchers he explained their use, evolvement and different features in lots of details. He has always been very nice and extremely helpful to students, no matter it's his student or a student from another department like me. I can never say too much thanks to him. Dr. Yang taught me biomaterial science, which was very helpful for this study. His homework and exams were composed of a good portion of independent thinking questions, which made me really digest what he taught in class and know how to use them.

I'm very grateful to work with my awesome lab mates. Thank Patricia and Koyal for patiently training me cell culture and other lab techs. Thank Scott and Michael for listening to my frustrations and discussing possible solutions with me. Thank Jenifer and Isaac for teaching me how to use JMP software. And thank Yali and Anlin for enlightening me on the better usage of the microscopes.

A special thanks to all my friends, especially Beata, Zhuo, and Xi. I came to Richmond all by myself and they gave me the most precious friendship and great support for my life. I love them. I also want to thank Dr. Joseph Feher from the Physiology Department and Dr. Colleen McLoughlin for their help on my TA job for my first year here. They are more than colleagues to me. They are my deeply respected and trusted friends.

This work is dedicated in love and gratitude to my parents. I know how much they would like me to stay at a closer city and see them more often. But when I told them I want to go to the opposite side of the earth for grad school, they still unconditionally supported me to go for my dream, both financially and emotionally. They were always there for me when I encounter difficulties in life and work. No any accomplishments could have been achieved without them.

Table of Contents

List of Tables

List of Figures

Abstract

PREPARATION AND CHARACTERIZATION OF A SELF-CRIMP SIDE-BY-SIDE BICOMPONENT ELECTROSPUN MATERIAL

By Yang Han, B.S.

A thesis submitted in partial fulfillment of the requirements for the degree of Master of Science in Biomedical Engineering at Virginia Commonwealth University.

Virginia Commonwealth University, 2012

Major Director: Gary L. Bowlin, PH.D,

Professor, Biomedical Engineering

Bicomponent composite fibers have been widely used in the textile industry and are gaining increasing attention on biomedical applications. In this research, polycaprolactone/poly (lactic acid) side-by-side bicomponent fibers were created for the application of a biodegradable scaffold. The side-by-side structure endowed the fiber with self-crimps when it was processed under certain conditions. This material was produced by electrospinning and collected on a high-

speed rotating mandrel to get highly oriented fibers. A mechanical stretch at the same direction was done followed by a wet heat treatment for polymer retraction. Crimped fibers were demonstrated by scanning electron microscopy. The quantitative porosity and uniaxial tensile strength was not affected by the post-treatments, but the cell ingrowth and proliferation after seeding the scaffold were significantly improved. In conclusion, the side-by-side crimped material serves as a better extracellular matrix analogue without sacrificing mechanical properties.

Introduction and Background

Organ transplantation has been clinically used for the replacement of damaged or absent organs. However, the organ supply is severely limited and many patients have to be put on a waiting list for a donor's organ. According to the "2010 Annual Data Report" from Organ Procurement and Transplantation Network (OPTN) and Scientific Registry of Transplant Recipients (SRTR), at the start of year 2009, 79,161 patients were on the kidney transplantation waiting list in the United States. By the end of the year, 16,830 patients accepted transplant while 5,412 patients died because they didn't get the transplantation in time and 1,475 became too sick to accept a transplant. At the same time, 33,215 new patients were added to the waiting list [1]. This is just one example of many organ donor shortage stories.

Engineered prostheses are designed to resolve this organ shortage crisis. Taking blood vessel implantation for example, synthetic materials such as polyethylene terephthalate (PET) and expanded polytetrafluoroethylene (ePTFE) are often used for the substitution of the patient's own vessel. However, synthetic materials do not always provide good patency rates, because their long term biocompatibility is limited [2]. Integrating living cells into scaffolds seems to be a better way to create implants. In the 1990s, Tissue Engineering was proposed as a new discipline of science and it holds a high potential to eventually solving the problem.

Tissue and Tissue Engineering

The human body functions normally with the cooperation of ten organ systems: skeletal, muscular, circulatory, nervous, respiratory, digestive, excretory, endocrine, reproductive, and immune. Each organ system is made up of two or more different organs. For example, the skeletal system includes bones, cartilage, tendons and ligaments, and the circulatory system is composed of the heart, blood vessels and blood. Organs are composed of repeating tissues that carry out a specialized physiological function. There are four traditional classes of tissues: epithelial, connective, muscle and nervous.

A tissue is an ensemble of cells and the extra-cellular matrix (ECM) in which they reside. ECM is composed of a large number of proteins and polysaccharides. It is synthesized and secreted by cells, and can be degraded by a family of enzymes called matrix metalloproteinases (MMP). ECM not only provides structural support to the cells, but also functions as a regulator and intermediary for the cells. It can regulate cell differentiation, apoptosis and migration [3]. Thus, the replication of this ECM is a critical component to any tissue engineering approach.

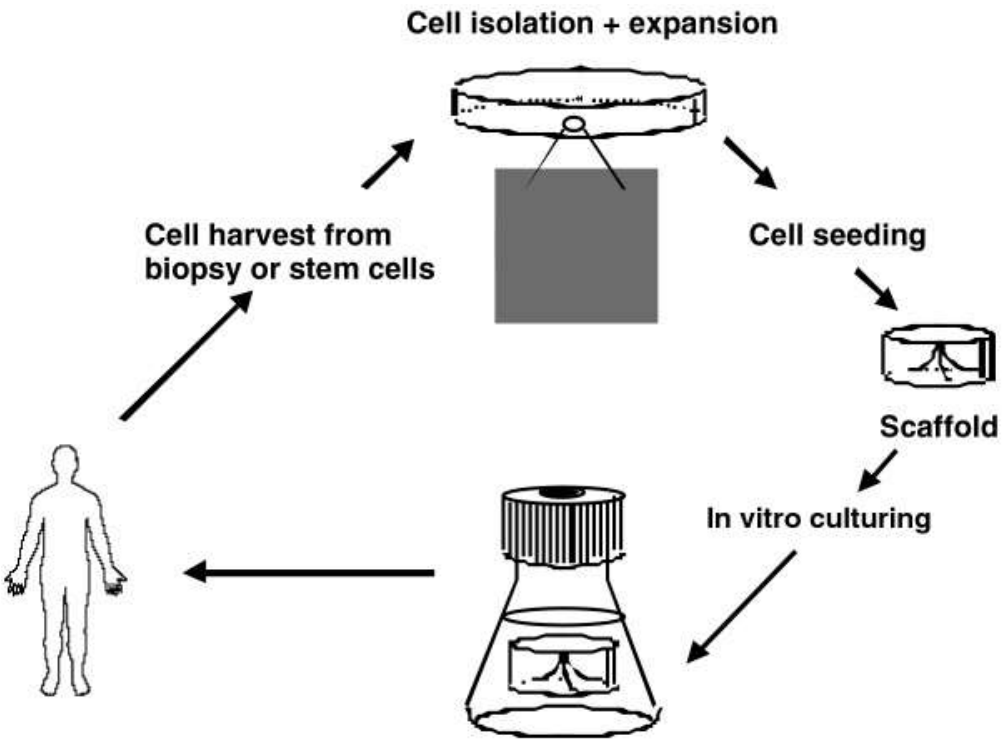

Figure 1. Concept of Tissue Engineering [4].

Tissue engineering aims at mimicking this composition of normal native tissues and creating substitute implants to solve the donor shortage problem. According to Langer and Vacanti, tissue engineering is "an interdisciplinary field that applies the principles of engineering and life sciences toward the development of biological substitutes that restore, maintain, or improve tissue function or a whole organ" [5]. The ultimate goal of tissue engineering is to make new organs that are implantable and compatible to human bodies. Under the stimulation of growth factors, isolated cells can attach to and proliferate on biomaterial matrices, eventually forming a living tissue (Figure 1). The ideal scenario is that the specific cells regenerate and make their own extracellular matrix on the biomaterial, gradually replacing the synthetic biomaterials.

Ideal Biomaterials for Tissue Engineering Scaffold

The biomaterial matrix for tissue engineering should possess proper mechanical and structural properties which are close to the replaced native tissue. This includes but is not limited to appropriate shape, dimensions, tensile, compression and shear modulus and strength, and anti-fatigue properties. The biomaterial should also interact well with its surrounding tissues and not induce severe immune responses from the host body. That is to say, it must be biocompatible. The surface of the matrix material needs to be suitable for cell attachment, proliferation and differentiation.

Porosity is among the most important characteristics for an ideal tissue engineering scaffold. High porosity can increase the specific surface area of a material, thus improving cell attachment. An interconnected network will help to promote cell/tissue growth and infiltration to form a three dimensional tissue. It not only provides the space for cells to proliferate, but also the tissue's revascularization. The newly generated vessels ensure nutrition supply and metabolic waste transport for the implanted cells, which is crucial for the cells' survival and regeneration of the new tissue [6, 7].

The implanted scaffold should degrade with time and be replaced by regenerated tissue. So far, many clinically used organ prostheses are not biodegradable, which is not good for the long-term biocompatibility. As mentioned previously, the clinically used vascular prostheses are made of PET and ePTFE textile. Their long-term patency rate as medium to large caliber arteries (>6mm) is close to autogenous materials [2, 8]. But for small-caliber vessels (<6mm), such as coronary arteries and infraninguinal arteries, the patency rate of synthetic vascular prostheses are

far worse than autovenous bypasses [9]. The reason of this phenomenon is because the prostheses materials are thrombogenic. In large-caliber vascular prostheses, the massive blood flow reduces the likelihood of proteins and cells attaching to the inner surface of vessel, thus thrombus incidence is brought down. While in small-caliber prostheses, the flow rate of blood is relatively low, giving a higher chance for proteins and cells in blood to anchor onto the inner surface of prostheses, this leads to thrombosis and eventually the failure of the implant [2]. The only known non-thrombogenic surface so far is an endothelial cell layer, which is the inner-most layer of native human vessels. So if the vascular prosthesis possesses or gains an endothelial layer before or shortly after the implantation, it will be more likely that the prosthesis will have a higher patency life.

Electrospinning

Electrospinning is an easy and efficient strategy to produce continuous polymer fibers with diameters of nano- to micrometer scale. At its most basic, it utilizes a high electric voltage field to extract fibers from a charged polymer solution, the solvent of which quickly evaporates, leaving only the solute polymer to form a continuous fiber. Figure 2 presents a basic electrospinning setup. Polymer solution is pumped at a specific speed from a syringe into a steel needle or spinneret. The needle is connected to a positive electrode with high voltage potential. A specific distance away from the spinneret is a grounded target which is used to collect fibers. At the tip of the spinneret, the droplet of solution is subjected to the strong electric field between the charged needle and the grounded target, and it is deformed into a cone of fluid named, the

Taylor cone. A liquid jet ejects from the Taylor cone downfield toward the grounded mandrel. After a period of linear elongation, the jet suffers an electrically-induced bending instability which results in a "whipping" motion of the polymer jet. Solvent evaporates from the jet during this whipping process and the strong looping stretches the polymer into an ultrathin fiber. The fiber is deposited on the grounded target as solid polymer to compose a nonwoven mesh of high porosity (~70%-90%) [10].

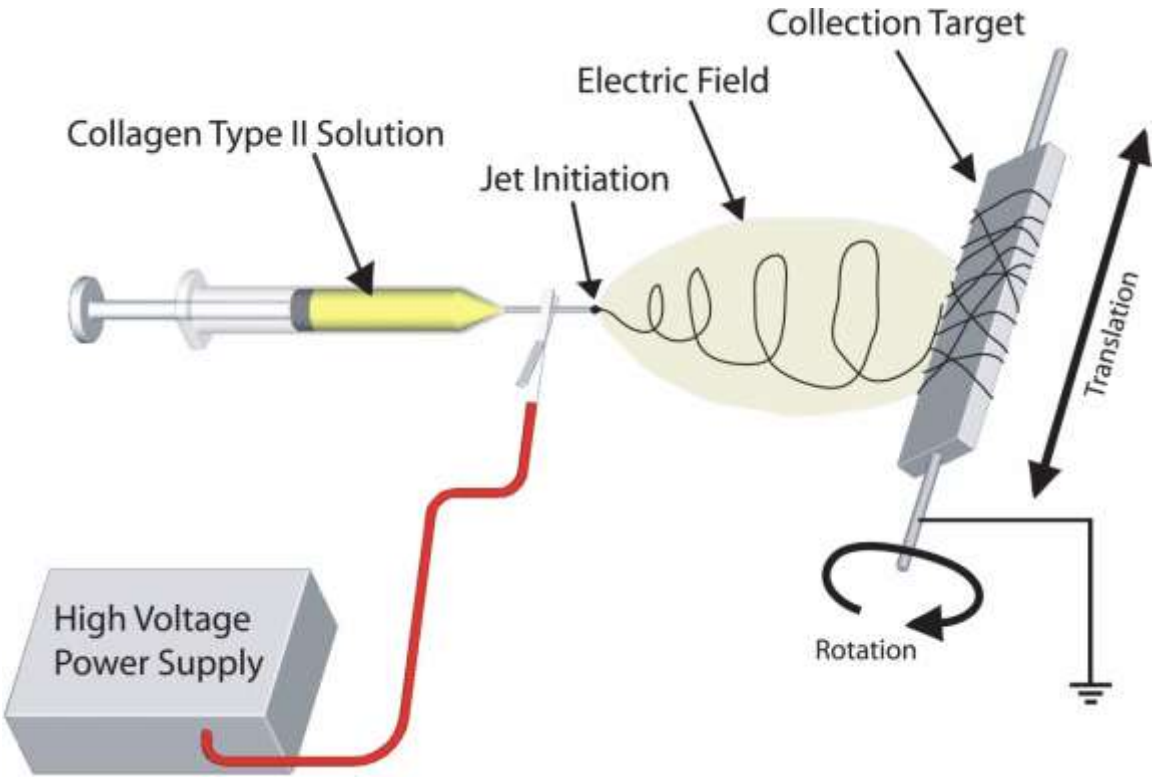

Figure 2. Schematic of the electrospinning process to illustrate the basic phenomena and process components [11].

Compared to the other methods of producing highly porous scaffolds, such as solvent casting and particulate leaching, gas foaming, emulsion freeze-drying, rapid prototyping, and

thermally induced phase separation [6], electrospinning is easier to process and of lower cost. Thus, it is the most promising method for commercial production of tissue scaffolds.

The process of electrospinning was first patented in the 1900s [12, 13]. In the 1960s Sir Geoffrey Ingram Taylor mathematically modeled the shape of the cone formed at the tip of fluid droplet [14 -16], and this is why that cone is named the Taylor cone. In the 1990s, several research groups demonstrated that many organic polymers could be electrospun into nanofibers [17]. Since then, electrospinning has gained increasing attention from labs around the world. Biodegradable materials are electrospun and their mechanical properties and interactions between the scaffold product and cells were investigated [18, 19]. The effect of electrospinning parameters and methods on product morphology, structure and mechanical properties were also intensely studied [20]. A number of new techniques were applied on electrospinning to produce novel products. Several examples are adding nanomaterials with polymer solutions, coating template nanofibers using chemical vapor deposition (CVD) and upward needleless electrospinning [21]. Regardless of the technique used, the main limitation that exists is the lack of electrospun scaffold porosity to allow cell infiltration.

Side-by-Side Bicomponent Fibers

Side-by-side (SBS) bicomponent fibers are fibers that have two different polymers or one polymer with two different molecular weights running side-by-side along the filaments. The invention of this fiber structure was enlightened by the structure of wool (Figure 3). The inner structure of a wool fiber is heterogeneous. The cortex of wool is composed of two different types

of cortical cells, orth- and para-cortical cells [22]. The two components attach tightly to each other and rotate helically along the longitudinal axis. Because the two proteins have different mechanical responses, each single filament has a pronounced tendency to coil [23 -26].

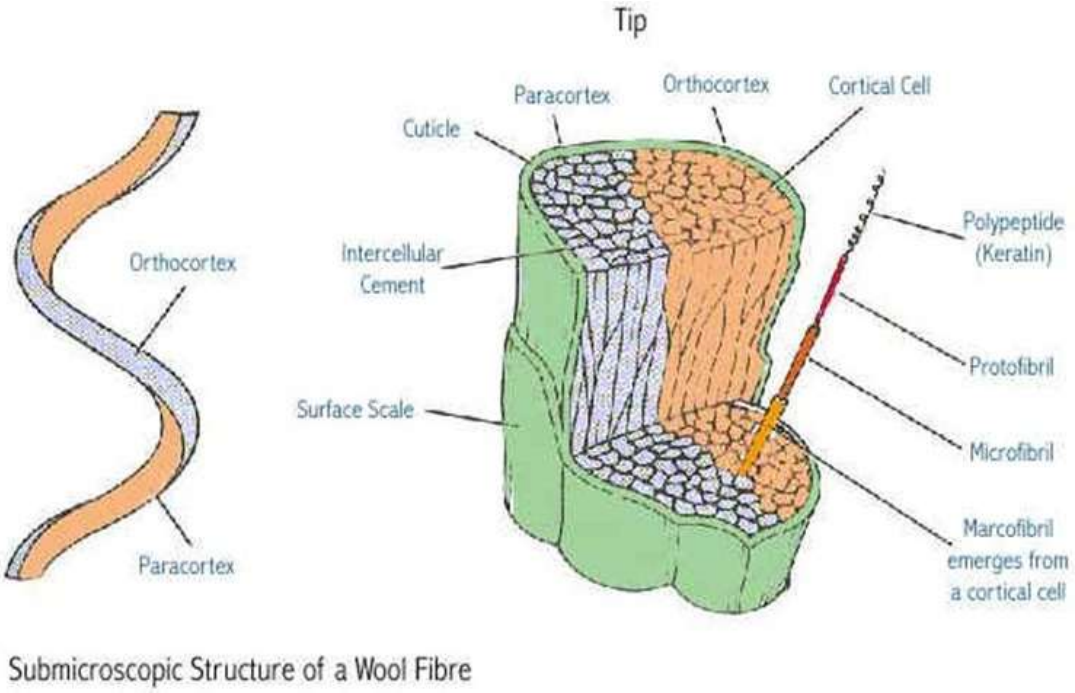

Figure 3. Submicroscopic structure of a wool fiber [22].

Bicomponent fibers have been commercially available since the 1960s, when DuPont™ produced a side-by-side hosiery yarn called "Cantrese". This yarn is made up of two nylon polymers which have different recoil rates. When the yarn retracts under certain conditions, one component shrinks more than the other, which pulls the filament to a permanent crimp. Thus, a highly coiled elastic fiber is formed [27]. Side-by-side bicomponent fibers have more crimps than as-spun fibers, thus are **highly porous** and stretchable.

The production bicomponent fibers by electrospinning have been studied by many labs. The fiber structures used include side-by-side, core-sheath and hollow structure, which can be considered as a modified version of core-sheath structure. In Liu's study, titanium dioxide (TiO_2) and SnO_2 were electrospun with a side-by-side dual spinneret. So both components can be exposed at the surface of the material, which can effectively reduce the recombination of photogenerated charge carriers [28]. Core-sheath structured electrospun fibers are the concentration of many bicomponent studies. Phenyleneethynylene oligomer mixed in dimethylformamide (DMF) with a poly(styrene-co-maleimide) (PSM) were electrospun in a core-sheath fashion and the product was proven to be fluorescent, which might be used as fluorescent sensors [29]. Hollow nanofibers were prepared by electrospinning two materials through a coaxial, two-capillary spinneret. Heavy mineral oil and an ethanol solution of poly(vinyl pyrrolidone) (PVP) was used as the core part and $Ti(OiPr)_4$ as the sheath. The electrospun product was then placed in octane overnight, so the mineral oil was extracted, leaving only the sheath part. These hollow fibers can be potentially used in fabricating fluidic devices and optical waveguides [30].

As for side-by-side bicomponent electrospinning, most researches were focused on getting the physical or chemical properties of both components, such as using a lower melting temperature component to spin-bond the other component, or using one component to enhance the effect of the other or cover the drawback of the other. But the research on the morphology and porosity properties which might be affected by the crimping characteristic of the fibers is not commonly seen. The influence of these factors on the cell-biomaterial interaction is not fully studied either.

Gupta and Wilkes used two platinum electrodes to penetrate into the syringes and charge the two polymer solutions. Two Teflon needles with two free ends adhered side-by-side were attached to the syringes. Here two polymer systems, poly (vinyl chloride)/segmented polyurethane (PVC/Estanew) and poly(vinyl chloride)/poly(vinylidiene fluoride) (PVC/PVDF), were tested for the electrospinning by this setup [31]. In this study, the potential of producing side-by-side bicomponent fibers was demonstrated, yet the product made by this device system was not always side-by-side along the length of the fibers. The crimping properties were not fully explored.

Lin et al. designed a micro-fluidic spinneret for side-by-side electrospinning. They used polyurethane (PU) and polyacrylonitrile (PAN) as the two components of the composite fiber. They briefly mentioned that if there is an electrical, chemical, physical or mechanical method to trigger the differential shrinkage of the two components, the fiber could be bent and be used as nanosensors or nanoactuators [32].

The aim of paper is to explore the method of creating a self-crimp side-by-side bicomponent fiber and evaluate the morphological, mechanical and biological properties of this new biomaterial. A simplified side-by-side spinneret was designed and two biodegradable fibers with different Young's Modulus, polylactide (PLA) and poly(ε-caprolactone) (PCL), were used as the two components of the bicomponent fiber. Micrographs were taken to prove that the fibers were a side-by-side structure, and then porosity was measured to test if there was an improvement on scaffold porosity. Human dermal fibroblasts (HDF) were seeded and cultured on the scaffold to test if the novel scaffold enhanced cell proliferation and infiltration. Tensile tests were also performed to examine the mechanical properties of the scaffold. The hypothesis was that SBS crimped scaffold will have a higher porosity and better cell infiltration.

Materials and Methods

Materials

The most widely researched biodegradable synthetic materials for tissue engineering are aliphatic polyesters, including polylactide (PLA), poly(glycolides) (PGA) and poly(ε-caprolactone) (PCL). They are extensively used as biomaterials because they are biodegradable and non-toxic to the human body [6]. In this study, PCL and PLA are chosen to be used as the two components of the side-by-side fiber. All reagents in this research were purchased from Sigma Aldrich Company if not specified otherwise.

Due to the chiral nature of lactic acid, PLA has three types of isomers: L, D, and DL isomers [33, 34]. The commercially available PLA polymers are the copolymers of poly-L-lactide (PLLA) and poly(D,L-lactic acid) (PDLLA) . The PLA used in this study is 100% PLLA. Its density is 1.23 g/cm^3. PLLA is highly crystalline and degrades very slowly. It is relatively hard with a glass transition temperature (T_g) at about 65 °C and melting temperature (T_m) of about 170-180 °C [34]. PLA is a very brittle at room temperature and thus plasticizers such as PCL are often added to improve its mechanical properties [35, 36].

PCL is a linear polymer composed of repeating monomers, so compared to PLLA it is softer. PCL's density is 1.14 g/cm^3. The glass transition temperature of PCL is around -60°C and

melting temperature is 58-63 °C. The degradation time of PCL is 2 years, which is relatively long. PLA is often added as a copolymer to PCL in order to reduce the degradation period [34].

PLA and PCL are chosen to be used in this side-by-side structure because their modulus and glass transition temperature is significantly different, which provide a potential of inducing differential shrinkage to the two sides of the bicomponent fiber. The different degradation periods of the two can also be potentially utilized to meet different requirements of the scaffold.

Electrospinning

According to earlier lab experiences [11], both PCL and PLA can be dissolved in 1,1,1,3,3,3-Hexafluoro-2-Propanol (HFP). PCL and PLA are separately dissolved in HFP. A concentration of 150 mg/mL is chosen for both PCL/HFP and PLA/HFP solution. Both solutions are agitated for 24 hours.

The experimental setup for bicomponent electrospinning was similar to that used for single-component electrospinning, except for the dual-spinneret assembly. The electrospinning apparatus consists of a syringe pump, a high voltage generator, a home-made needle spinneret, and a rotating mandrel (Figure 4). PCL/HFP solution and PLA/HFP solution were separately loaded into two 3 ml Becton Dickinson syringes, each of which is capped with a 21 gauge blunt-tipped needle. Each needle was connected to a Tygon® S-54-HL medical tubing (Part Number AAQ04119, Norton Performance Plastics Co.). The homemade spinneret setup (Figure 5) was attached to the other end of the tubing and directs the two solutions into a side-by-side pattern. The spinneret was made up of two bent 21G needles tied together, the needle tips face-to-face to

ensure the encountering of the two droplets at the middle. A KD Scientific syringe pump (Model 100) drives each syringe at a rate of 1.8 mL/h. A high voltage generator (Spellman CZE1000R; Spellman High Voltage Electronics Corporation) provides a voltage of 25 kV to the spinneret. The distance between the tip of the side-by-side spinneret and the grounded target mandrel was set as 25 cm. So the electric field was 1 kV/cm between the spinneret to the mandrel. The mandrel was a 37 mm × 37 mm × 5mm stainless steel. The mandrel rotated at a rate of 2710 rpm, which corresponds to a linear speed of 5.25 m/s. This high rotating speed gave the bicomponent fiber a relatively high internal stress along the longitudinal direction, which will later help to form the crimp effect along fibers. Immediately after electrospinning, scaffolds were cut from the mandrel and placed in a fume hood for overnight degassing and removal of remaining HFP.

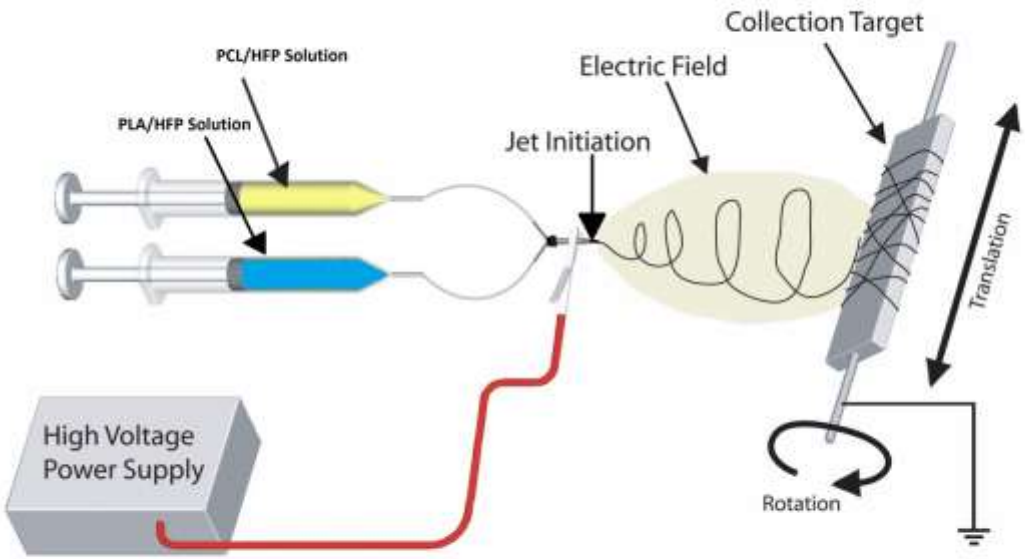

Figure 4. Electrospinning setup for side-by-side bicomponent material.

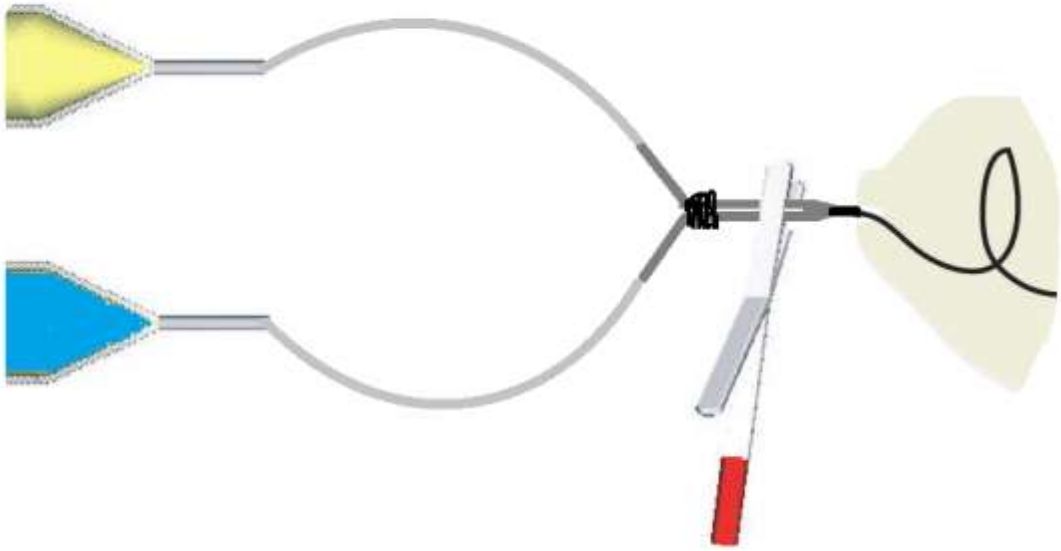

Figure 5. Side-by-side bicomponent spinneret.

During electrospinning, a single Taylor cone was observed extruding from the middle of the joined droplet. This proves that the polymer solution have a single jet composed of PLA and PCL. Another study which used a similar setup also reported the formation of side-by-side structure (Figure 7) [37].

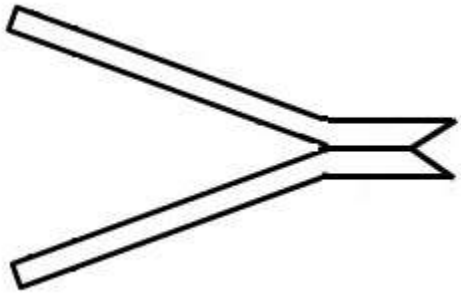

Figure 6. Illustration of face-to-face needles used to create side-by-side fibers.

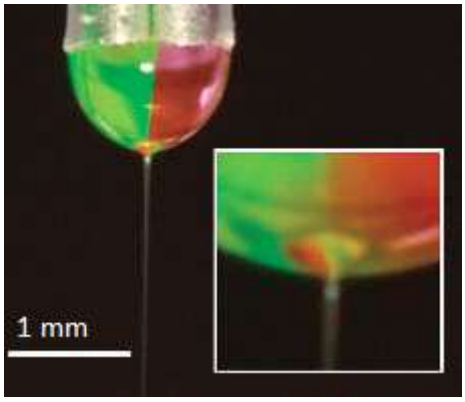

Figure 7. Electrospinning of two PEO/distilled water (2% w/v) solutions each mixed with two fluorescent dyes. Left side: isothiocyanate-conjugated dextran (green); Right side: rhodamine-B-conjugated dextran (red). A well-structured side-by-side Taylor cone was observed at the tip of the nozzle, consisting of two aligned fluid phases [37].

Scaffold Processing

There were four groups of samples in total. Each group had three repeating scaffolds. For the experimental group (EX Group), 21 gauge needles were used in the electrospinning setup as shown in Figure 4. PLA and PCL fibers were electrospun in a side-by-side pattern. The scaffold was stretched along the fiber alignment direction on the mandrel by 80% at 24 °C (room temperature) for 1 hour. Then it was released to its free state and was soaked in 48 °C deionized water bath for 10 minutes.

For Control Group I (CI Group), the scaffold was electrospun from two separated 18 gauge needles and all other spinning parameters and scaffold post-treatments were the same as

EX Group. That is, the scaffold was stretched by 80% at 24 °C for 1 hour, and then released to free state and went through the wet-heat treatment in 48 °C deionized water bath for 10 minutes. For Control Group II (CII Group), the samples were just the scaffold directly from 21 gauge side-by-side electrospinning with no post-process.

For Control Group III (CIII Group), the samples were from 21 gauge side-by-side electrospinning and stretched by 80% at 24 °C for 1 hour, with no water bath afterwards.

All four groups of samples were left in a desiccation chamber overnight to ensure that they were completely free of moisture.

The 18 gauge needles used for CI Group had an inner diameter 0.838 mm. The other three groups are electrospun via 21 gauge needles, the inner diameter of which was 0.514 mm. Among the available standardized needles, gauge 18 was close to twice the inner diameter of gauge 21[38]. This is why gauge 18 was chosen to be used in CI Group.

SEM Morphology

The dry samples from each of the four groups were gold sputter-coated (Model 550; Electron Microscope Sciences) and then photographs taken by a scanning electron microscope (JSM-820 JE Electron Microscope; JEOL). Pictures of magnification 500× were taken to reveal an overall fiber morphology. The crimps can be examined via these micrographs. Another photograph of 5000× magnification was also taken for each group. In these micrographs, the single fiber structure were analyzed.

Scaffold Porosity Measurement

The hypothesis at the beginning of this research was that if this side-by-side bicomponent fiber scaffold is stretched along the fiber axial direction and then processed through a wet-heat treatment, PCL will recoil more than PLA, resulting in the scaffold gaining self-crimps and becoming more porous.

$$\text{Void Fraction} = 1 - \left[\frac{Calculated\ scaffold\ density}{Known\ material\ density} \times 100\%\right]$$

Void fraction was used as a measurement for porosity [39]. Since PCL and PLA dissolved in HFP with the same weight/volume concentration, and the pumping rate for the two are also the same, the weight percentage of PCL and PLA should both be 50%. The density of bicomponent material should be the average of the two components, which was calculated to be 1.19 g/cm^3.

"Dog-bone" shaped (2.75 mm wide at their narrowest point) samples were punched from each scaffold. Two dog-bone samples were taken from each of the three scaffolds of each group. So in total 24 dog-bones were tested. These samples were first used for porosity testing and then for the uniaxial tensile test. The surface area of the dog-bone shape was calculated to be 90.17 mm^2. The thickness and weight of each dog-bone sample were measured.

Uniaxial Tensile Test

To save materials, the dog-bone shaped samples from the porosity test were reused for this test. The samples were setup on a MTS Bionix 200 testing system (MTS Systems Corp.). The gage length was set as 7.5 mm and the load cell was 50 N. The samples were elongated at an extension rate of 10.0 mm/min until they fail. Peak load, peak stress, modulus, strain at break and the energy consumed to break the sample were calculated by the MTS software TestWorks 4.0 and recorded.

Cell Response Test

In order to evaluate the influence of SBS fiber structure on cell-scaffold interaction, human dermal fibroblasts (Cascade Biologics) were seeded and cultured on each scaffold. HDFs were cultured in flasks in a 37 °C and 5% CO_2 incubator. The media was composed of DMEM-F12 medium supplemented with 10% fetal bovine serum and 1% penicillin-streptomyocin. When the cells were confluent in the flask, the HDFs were harvested and put into a small amount of media. The cell suspension was diluted to a concentration of 4 million cells per milliliter.

Three 10 mm round diameter discs were punched from each group of samples. They were soaked in ethanol for 30 min, and then rinsed in phosphate buffered saline (PBS) for 10 minutes for three times. The disinfected discs were placed in a 48-well plate. A disinfected 10 mm cloning ring was put in each well to press the edge of the scaffold disc and make it stay at the bottom of well. 50 μL of the 4×10^6 cells/mL HDF suspension was first put on each 10 mm disc

and then incubated for 1 hour, so that the cells can attach to the surface of scaffold. Then 450 μL more media was added to each well. The initial cell culture concentration for each 10 mm disc was 2×10^5 cells/well.

After culturing the cells on scaffold for 1 day, 7 days, and 14 days, the scaffold discs were taken out of the plate and fixed in 10% formalin overnight. They were then processed for cryosection and were cut into 40 μm thick slices to expose the cross-sectional area. 1 μg/mL DAPI (4',6-diamidino-2-phenylindole) stain was used to stain the scaffold. The fixed cells can be dyed into fluorescent blue which is visible under UV light. A Nikon® Eclipse TE300™ fluorescent microscope was used to take the 100× sample images under both natural light and UV light. Two pictures from the two light conditions were integrated together using Photoshop®.

Statistical Analysis

The results of porosity test and tensile test were analyzed via JMP® PRO 10 statistical software package (SAS Institute). Firstly, a Kruskal-Wallis one-way analysis of variance (ANOVA) was used to compare and see if specific test results of all groups had the same population mean. Then a Tukey-Kramer pairwise multiple comparison procedure ($\alpha = 0.05$) was performed to find the significant differences on the population mean of all possible pairs of the four groups. Graphical depictions were constructed with Microsoft Excel 2010, with error bars representing standard deviations.

Results

SEM Morphology Test

The SEM micrographs (500×) of each group of samples are shown in Figure 8. Comparing the SBS scaffolds (CII, CIII and EX Group), it can be clearly seen that the untreated fibers (CII) are fairly oriented and present a straight form along the mandrel rotating direction. After 80% stretching for 1 hour, the diameters of fibers became thinner and possessed a wavy morphology rather than staying straight (CIII). This is because upon releasing from the stretch, fibers naturally recoil. After the wet-heat treatment (EX), the fibers gain more dramatic crimps and become thicker. This is very likely to be caused by the shrinkage of PCL.

The fiber diameters in CI are about the same size as the EX Group. This is because the cross section area of two 21 gauge needles tying side-by-side add up to a similar cross section area of a 18 gauge needle, so both type of fibers come out from a similar size of droplet. In this case, the Taylor cone formed from the two droplets should have similar physical dimensions, thus producing a similar sized fiber. So each fiber shown in the CI picture was a single component fiber while each fiber seen in the EX picture was a bicomponent fiber (Figure 8).

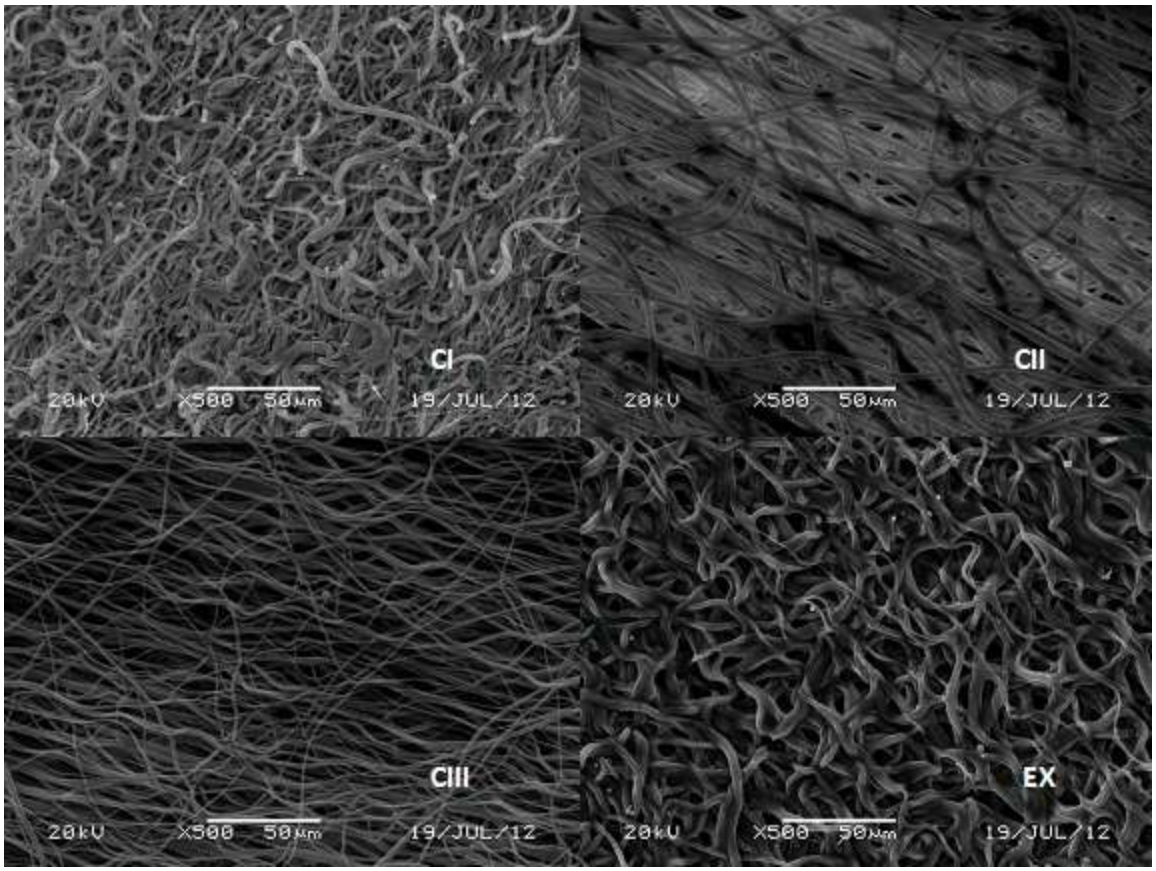

Figure 8. SEM micrographs taken at a 500× magnification.

Fibers in CI possess some crimps but this weaving deformation is rather uneven: only happens to some of the fibers. The scaffold surface looks flat overall. Considering each fiber in CI has only one polymer component, it is reasonable to predict that the crimping fibers are PCL and straight fibers are PLA. The existence of large number of straight PLA fibers makes the scaffold have rather small pore sizes. In comparison, the crimps are more significant and more of a common phenomenon among fibers in the EX group. Fibers are curled in a three-dimensional manner. This demonstrates the hypothesis that electrospun SBS fibers can gain crimps if treated with appropriate processes.

The representative pore shapes for CI, CII and CIII scaffold are longitudinal and oriented, while pores in EX scaffold are diversified and well-rounded. This might lead to a result that the EX scaffold is more isotropic than the other three group. But this was not specifically tested in this study.

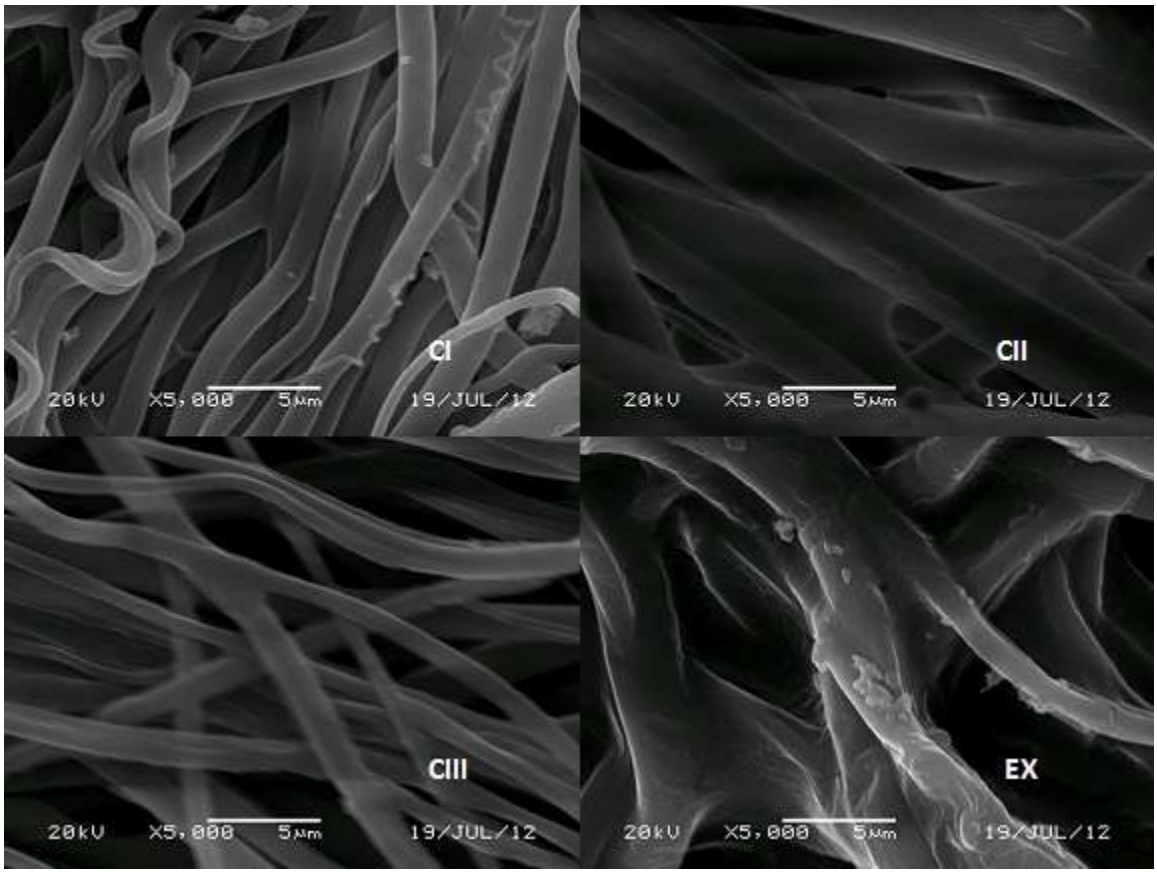

Figure 9. SEM micrographs taken at a 5000× magnification.

The SEM micrographs (5000×) of the samples are shown in Figure 9. The side-by-side structure can be seen from CI and CII Groups. In EX Group the fibers can still be seen to be bonding together, and the pores are very distinct. In CI Group, straight fibers are oriented and close to each other.

There are some bonded spots between fibers in the EX Group, and this can be observed from both low magnification (Figure 8) and high magnification micrographs (Figure 9). The bonded spots are possibly caused by the softening of PCL during wet-heat treatment. Although PCL's melting point is 58-63 °C, being micro- to nanometer scale the PCL fibers are possible to become unstable at a lower temperature like 48 °C.

Scaffold Porosity Measurement

Three scaffolds of each group were made for testing. Two dog-bone punches were taken from the each scaffold. The original data is shown in Table 1.

The void fraction of CI is significantly different from the other three groups. Void fraction of CI is lower than EX Group. This confirmed what is observed in the SEM micrographs (Figure 8 and 9): CI fibers are tightly aligned and EX fibers crimps and has higher porosity. The porosity of CII, CIII and EX Groups are not significantly different, which is inconsistent with the initial prediction of the experiments. One possible reason is that the non-treated SBS electrospun scaffold (CII Group) has a quite high porosity (mean value 82.90% with standard deviation of 0.99%) already. The 80% elongation for 1 hour is not going increasing the porosity significantly on this high porosity basis.

Table 1: Original Porosity Test Data

Sample Name		Thickness (mm)	Calculated Volume (mm^3)	Weight (g)	Calculated Density (g/cm^3)	Void Fraction (%)
Control Group I	CI-1-1	0.10	9.0170	0.0060	0.6654	44.08%
	CI-1-2	0.16	14.4272	0.0070	0.4852	59.23%
	CI-2-1	0.35	31.5595	0.0127	0.4024	66.18%
	CI-2-2	0.41	36.9697	0.0136	0.3679	69.09%
	CI-3-1	0.33	29.7561	0.0109	0.3663	69.22%
	CI-3-2	0.32	28.8544	0.0107	0.3708	68.84%
Control Group II	CII-1-1	0.34	30.6578	0.0063	0.2055	82.73%
	CII-1-2	0.27	24.3459	0.0053	0.2177	81.71%
	CII-2-1	0.22	19.8374	0.0039	0.1966	83.48%
	CII-2-2	0.13	11.7221	0.0025	0.2133	82.08%
	CII-3-1	0.18	16.2306	0.0033	0.2033	82.91%
	CII-3-2	0.18	16.2306	0.0030	0.1848	84.47%
Control Group III	CIII-1-1	0.14	12.6238	0.0021	0.1664	86.02%
	CIII-1-2	0.20	18.0340	0.0023	0.1275	89.28%
	CIII-2-1	0.24	21.6408	0.0048	0.2218	81.36%
	CIII-2-2	0.22	19.8374	0.0047	0.2369	80.09%
	CIII-3-1	0.18	16.2306	0.0035	0.2156	81.88%
	CIII-3-2	0.29	26.1493	0.0045	0.1721	85.54%
Experimental Group	EX-1-1	0.26	23.4442	0.0051	0.2175	81.72%
	EX-1-2	0.21	18.9357	0.0043	0.2271	80.92%
	EX-2-1	0.29	26.1493	0.0096	0.3671	69.15%
	EX-2-2	0.22	19.8374	0.0065	0.3277	72.47%
	EX-3-1	0.20	18.0340	0.0053	0.2939	75.30%
	EX-3-2	0.08	7.2136	0.0024	0.3327	72.04%

Table 2: Calculated Porosity Data.

Sample Name	Control Group I	Control Group II	Control Group III	Experimental Group
Mean Void Fraction	62.77%	82.90%	84.03%	75.27%
Standard Deviation	9.92%	0.99%	3.50%	5.08%

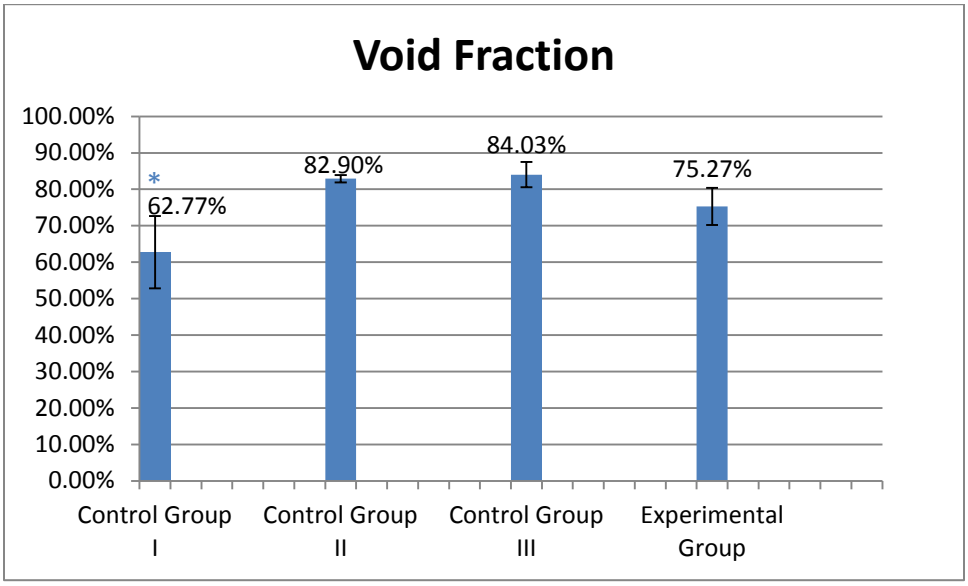

Figure 10. Mean void fraction of each group with standard deviations as error bar. (*) denotes statistical difference ($p<0.05$) from the other three of groups.

The void fraction standard deviation for the EX Group is 9.92%, which is much higher than CI (5.08%) and CII Group (3.50%), which are higher than CII Group (0.99%). The excess stretching and wet-heat treatments account for the bigger fluctuation in void fraction because (1) the fiber deformation during stretching might be uneven along the scaffold. Especially since the scaffold is not deposited perfectly evenly on mandrel during electrospinning, which is inevitable during the collection, the unevenness may be amplified during stretching; (2) during wet-heat treatment the polymers might also shrink or even degrade to different extent, which could render the result samples to have different porosities too.

Uniaxial Tensile Test

The original data of the uniaxial tensile test were shown in Table 3. The mean value and standard deviation of peak load, peak stress, modulus, strain at break and energy to break for each scaffold group is listed in Table 3.

Table 3: Original Data from Uniaxial Tensile Test.

Sample Name		Peak Load (N)	Peak Stress (Mpa)	Modulus (Mpa)	Strain At Break (mm/mm)	Energy To Break (N*mm)
Control Group I	CI-1-1	2.867	10.550	244.916	2.352	43.002
	CI-1-2	4.177	9.515	249.355	3.134	87.490
	CI-2-1	8.117	8.442	159.516	1.054	54.369
	CI-2-2	9.854	8.784	144.467	1.688	101.529
	CI-3-1	7.759	8.566	189.830	1.579	78.589
	CI-3-2	7.380	8.406	150.528	1.855	84.022
Control Group II	CII-1-1	1.919	2.056	19.938	1.766	20.715
	CII-1-2	1.494	2.023	21.362	2.586	24.075
	CII-2-1	1.865	3.077	42.261	1.570	17.438
	CII-2-2	1.042	2.931	60.763	1.697	11.376
	CII-3-1	1.111	2.246	263.517①	1.277	8.914
	CII-3-2	1.107	2.238	43.464	1.385	9.880
Control Group III	CIII-1-1	1.163	3.035	20.021	1.202	8.616
	CIII-1-2	1.455	2.644	16.815	1.239	11.028
	CIII-2-1	2.982	4.533	39.563	0.840	15.485
	CIII-2-2	3.052	5.034	60.716	0.607	11.468
	CIII-3-1	2.113	4.271	34.602	1.368	17.923
	CIII-3-2	3.914	4.927	32.932	1.622	37.720
Experimental Group	EX-1-1	1.566	2.203	21.258	1.313	12.297
	EX-1-2	1.644	2.844	37.351	1.796	18.555
	Ex-2-1	5.398	8.905	173.086	1.241	42.503
	Ex-2-2	3.165	8.259	84.906	1.046	20.192
	Ex-3-1	2.882	5.235	96.601	1.204	22.400
	Ex-3-2	1.978	9.156	126.228	0.932	11.276

①: The modulus of sample CII-3-1 in Control Group II is an outlier. It was removed while doing the data analysis.

Table 4: Calculated Data from Uniaxial Tensile Test.

Sample Name		Control Group I	Control Group II	Control Group III	Experimental Group
Peak Load (N)	Mean	6.692	1.423	2.447	2.772
	Stdev	2.630	0.397	1.053	1.444
Modulus (Mpa)	Mean	9.044	2.429	4.074	6.100
	Stdev	0.843	0.457	1.002	3.111
Energy To Break (N*mm)	Mean	189.769	75.218	34.108	89.905
	Stdev	47.115	93.505	15.728	56.183
Peak Stress (Mpa)	Mean	1.944	1.714	1.146	1.255
	Stdev	0.719	0.465	0.367	0.299
Strain At Break (mm/mm)	Mean	74.834	15.400	17.040	21.204
	Stdev	21.924	6.267	10.668	11.323

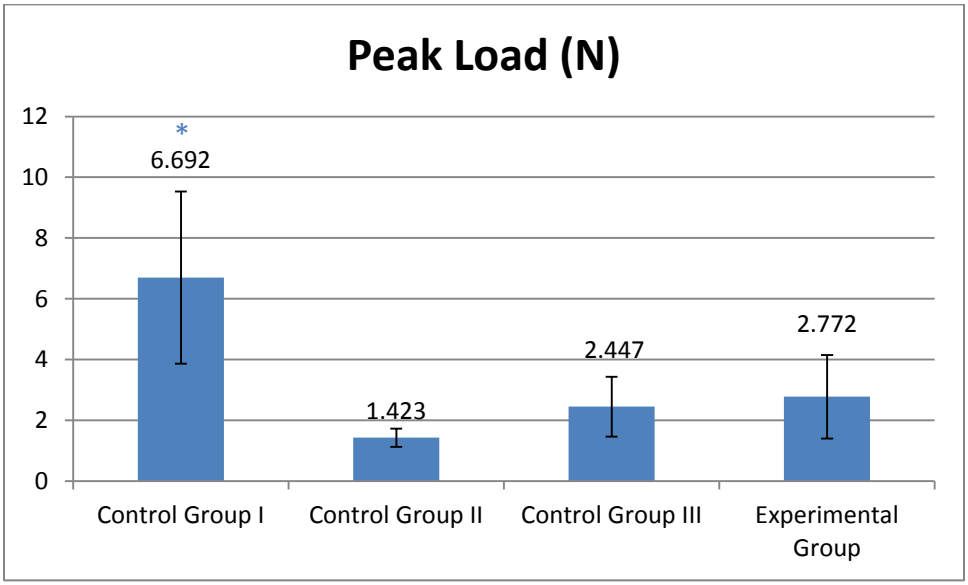

Figure 11. Mean peak load of each group with standard deviations as error bar. (*) denotes statistical difference ($p<0.05$) from the other three groups.

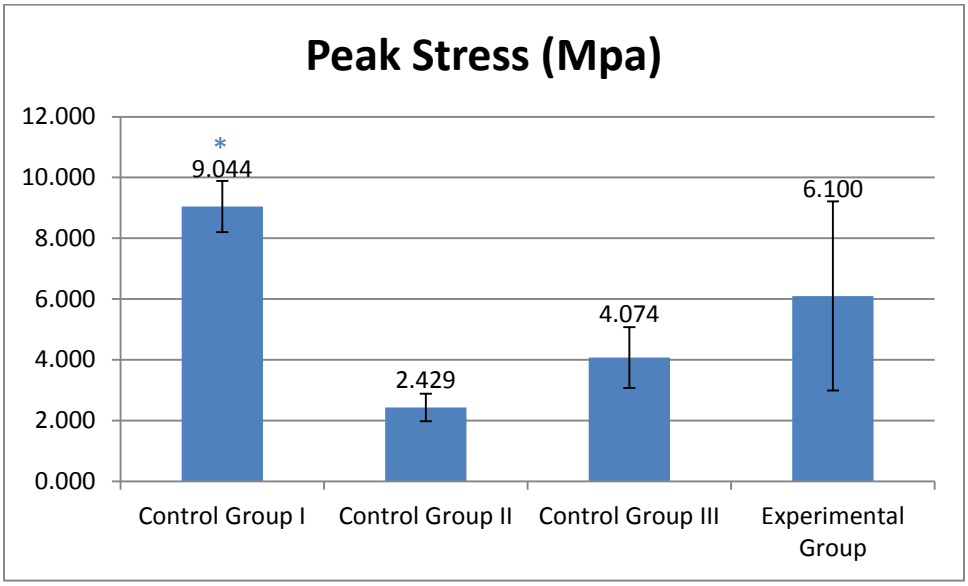

Figure 12. Mean peak stress of each group with standard deviations as error bar. (*) denotes statistical difference ($p<0.05$) from the other three groups. CII and EX are statistically different ($p<0.5$) from each other.

Figure 10 and 11 illustrates the peak load and peak stress of each group. The comparison between peak loads is not accurate to describe the differences between the groups, because the thickness of each sample was not exactly the same. Even if two samples are made of the same material, thicker samples would bear a higher peak load than a thinner one. So here the analysis is emphasized more on the peak stress.

Both peak load and peak stress of CI is significantly higher from the other three groups. Considering CI has single component fibers whose diameter is about the same with a two component fiber in the SBS groups, it is reasonable to extrapolate that a single component fiber can have a higher peak stress than a SBS fiber. Further discussion on this will be continued in the next chapter. In practice, not all fibers coming out from the SBS spinneret end up being a SBS fiber. On the other hand, those fibers who were electrospun as SBS structures might later split

during post treatments, depending on how tight the connection between the two fibers was. From the 5000× SEM micrographs (Figure 9), we can still find some non-SBS fibers in CII and CIII, and this also indicated this problem. So the average fiber diameter in EX is very likely to be lower than CI. This also contributes to the lower peak stress in SBS groups. Another reason that might also cause the higher peak load/stress of CI is its significantly lower void fraction. Being a denser fibrous scaffold than the other three groups, CI logically bears a higher peak load/stress.

The peak stresses of EX is significantly higher than CII. This is an improvement of the scaffold after the post processing. No significant difference is found between CII and CIII or CIII and EX. From this result, we can conclude that both stretching and wet-heat treatments are needed to improve the tensile stress of the scaffold. Neither of these two processes is sufficient enough to make a difference on the tensile stress of a scaffold.

The error bars of both peak load and peak stress of CII, CIII and EX show a tendency of increasing. This comes along with the fact that these three groups sequentially got more treatments, which could induce more random factors. This is a comparable theory as analyzed in the porosity test. Similar stories can be seen in Figure 13 and 14 for the Young's Mudulus and Break Energy.

The elastic modulus of CI is significantly higher than the SBS groups. This might attributes to thicker average fiber diameter and higher density of CI, as analyzed above. There is no statistical difference between CII, CIII and EX Groups.

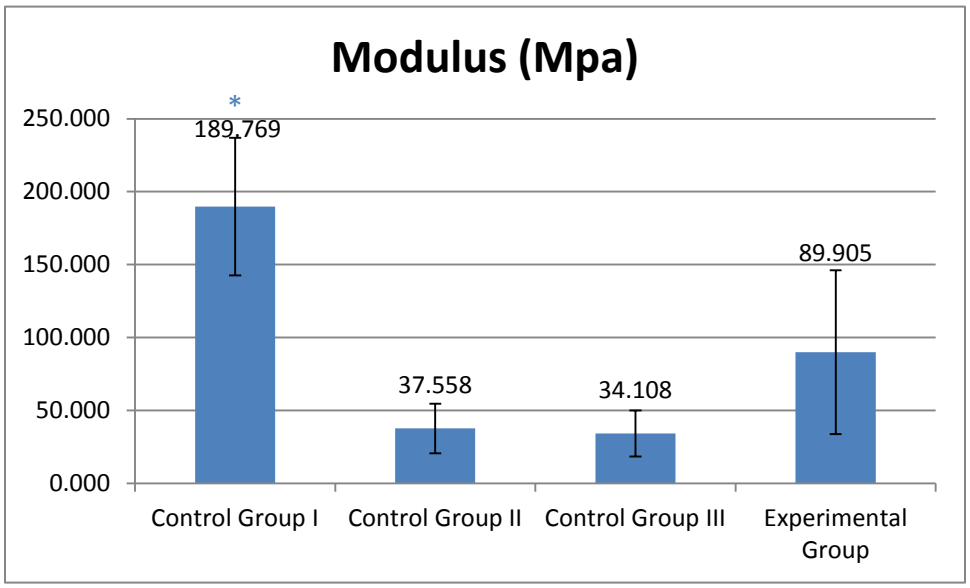

Figure 13. Mean modulus of each group with standard deviations as error bar. (*) denotes statistical difference ($p<0.05$) from the other three groups.

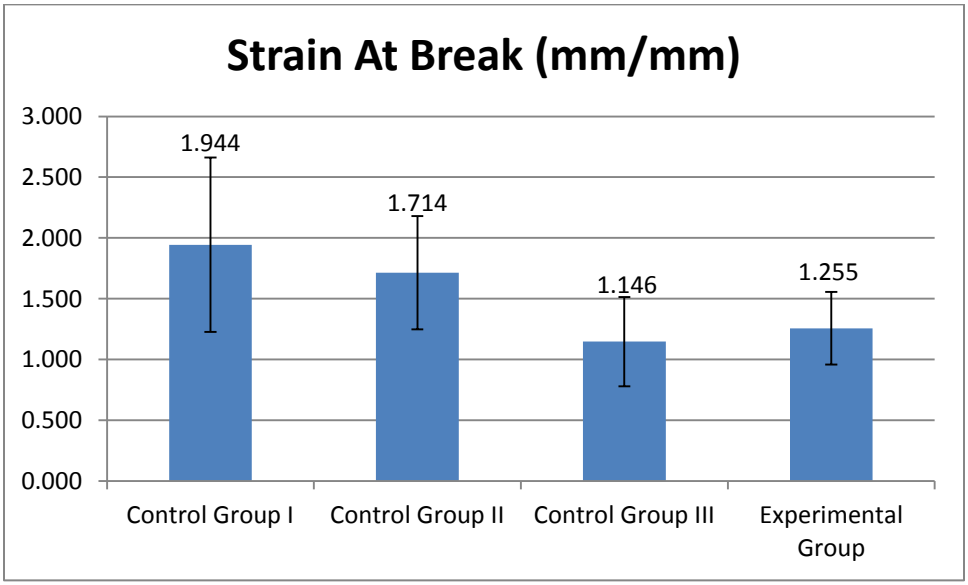

Figure 14. Mean strain at break of each group with standard deviations as error bar. CI group is statistically different ($p<0.05$) from CIII group.

The strain at break data (Figure 14) shows no significant differences between any pair of groups other than CI and CIII. This parameter is the maximum deformation rate of the scaffold. This maximum strain of EX was expected to be significantly higher than CII and CIII, because the SBS fibers in EX was predicted to be highly recoiled and very elastic. But this is not indicated by the Tukey-Kramer statistic test. This might be caused by the previously mentioned melting spots formed on EX scaffolds. Now that the EX fibers are connected at those spots, the elasticity of the whole scaffold will not be as high as expected. Thus the strain at break is reduced.

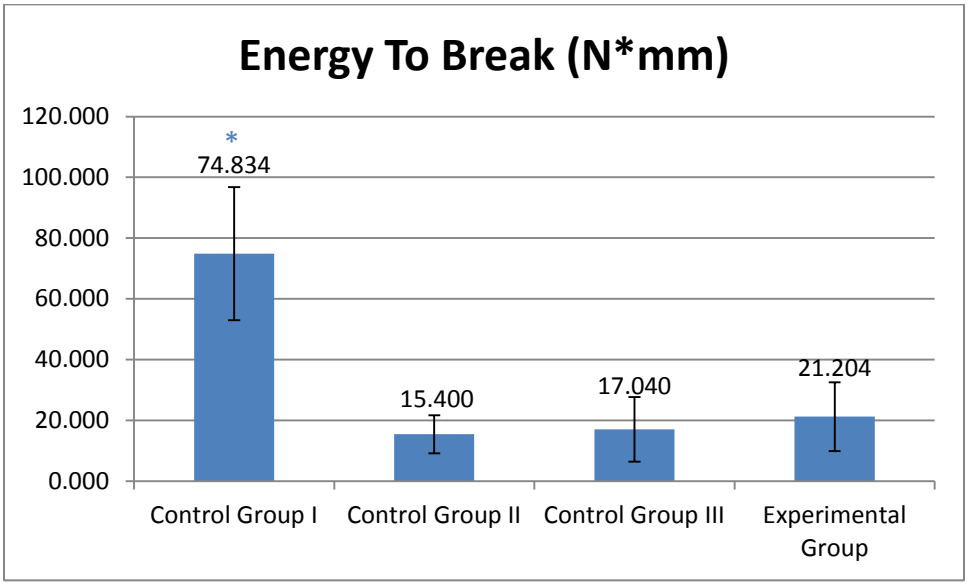

Figure 15. Mean energy to break of each group with standard deviations as error bar. (*) denotes statistical difference ($p<0.05$) from the other three groups.

The breaking energy of CI group is significantly higher than the other three. As discussed in the peak stress part, this might also be caused by the fiber diameter and void fraction difference.

Cell Response Test

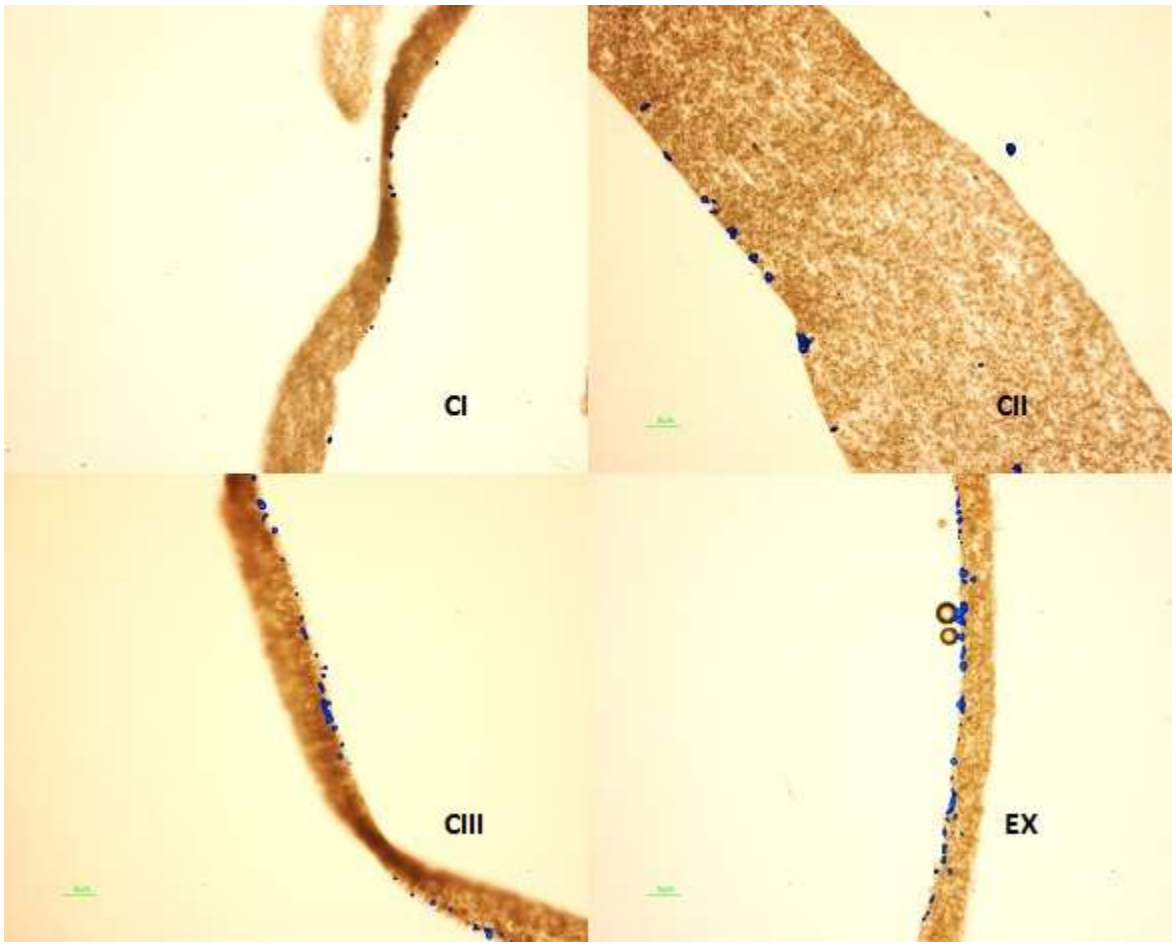

Figure 16. Micrographs of four groups of scaffolds after culturing cells for 1 day (100×). The blue dots are the dyed HDF cells.

The scaffold shown in each micrograph is 40 μm thick cross-sections of the scaffolds. So the width of each scaffold slice in the pictures is the thickness of the round scaffold discs. It seems that the disc thicknesses of the samples are not all the same. This is attributed to three reasons. Firstly, the thicknesses of each group are inherently different because they went through

different processes. CIII was stretched and should be thinner than CII. During heat treatment scaffold might shrink so CI and EX scaffolds are supposed to appear thicker than CIII. Yet this rule is not strictly followed because of the following two additional reasons. As a minor reason, the effective fiber deposition during the electrospinning of each scaffold is different. Due to the systematic drawback of the electrospinning equipment, it is hard to control the electric field. Sometimes polymers can be drawn into metal parts of the setup, instead of being attracted to the mandrel. When this happens more severe, the scaffold product ends up being thinner than the others because fewer polymers are collected on the mandrel. Furthermore, even in a single scaffold disc sample, the thickness is inconsistent and even dramatically different. Different width scaffold slices from the same scaffold were observed under the microscope.

After the first day of culture, the cells attached to the surface of scaffolds. The stretched scaffold (CIII) and fully-processed scaffold (EX) already show better cell attachment than the other two (Figure 16). After 7 days, only a few cells migrated through the thickness of the scaffold discs in CI, CII and CIII Groups. A prominent amount of cells migrated through the EX scaffold and reached half way over its cross-section. 14 days later, cells of CI Group only remained attaching on the surface and near-surface area. On the untreated SBS scaffold (CII), cells mainly proliferated at the surface of scaffold and only a minority of them migrated into the cross section of the scaffold. Whereas in the stretched scaffold (CIII) and fully-treated scaffold (EX), the cell migration was throughout the whole cross section and presented a rather even distribution. No major proliferation on the scaffold surface was observed.

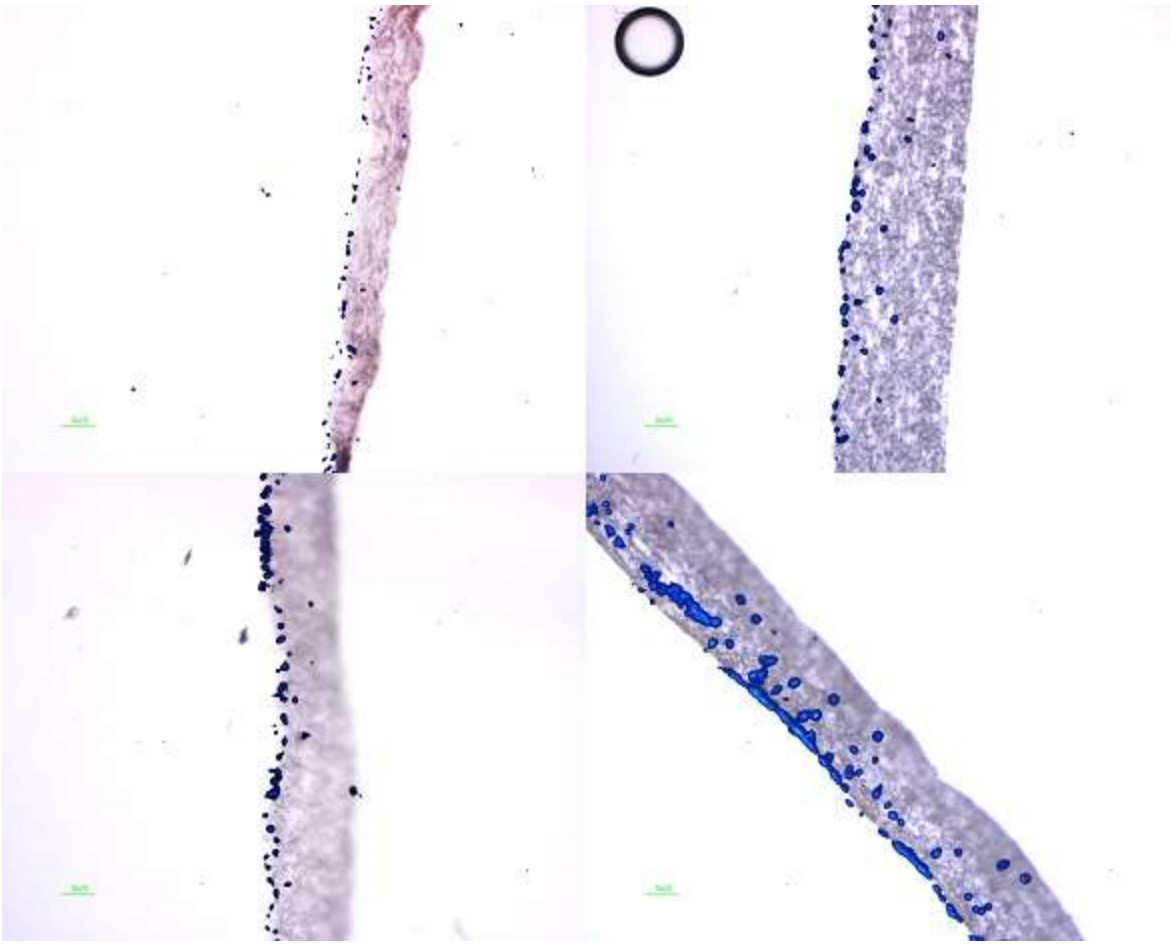

Figure 17. Micrographs of four groups of scaffolds after culturing cells for 7 days (100×). The blue dots are the dyed HDF cells.

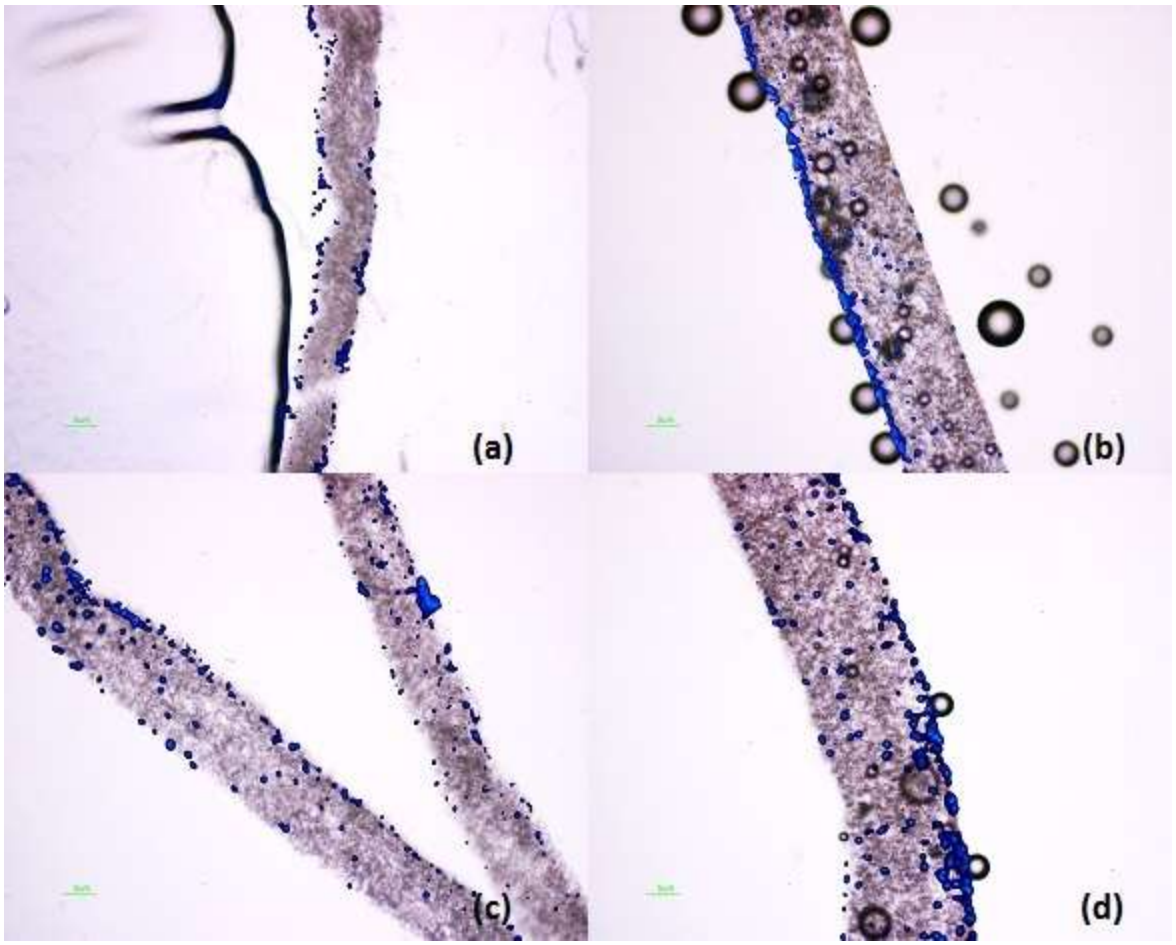

Figure 18. Micrographs of four groups of scaffolds after culturing cells for 14 days (100×). The blue dots are the dyed HDF cells.

Discussion

Electrospinning Process of SBS fibers

As mentioned previously, customized spinnerets are used in the textile industry to extrude side-by-side fibers (Figure 5). Considering that the polymer jet forms from the Taylor cone, not directly from the needle/spinneret tip, the substitute of side-by-side tied needles to a customized spinneret is reasonable. During the electrospinning process, droplets from two needles fused together and a single Taylor cone was formed at the tip of fused droplets. Thus theoretically a side-by-side structure should be seen in electrospun fibers. The SEM micrographs also proved the success of this home-made spinneret.

In Lin's research mentioned the first chapter, a "microfluic" spinneret was used for SBS electrospinning (Figure 19). Three 0.630 mm diameter stainless steel rods were glued together with commercial cyanoacrylate glue to form the channels in the spinneret. After casting by silicone elastomer with a plastic mold, two silicone tubes were connected to the two side channels for the delivery of the two polymer solutions. A 20 gauge stainless steel needle tip was inserted to the common channel and served as the tip of the spinneret [32].

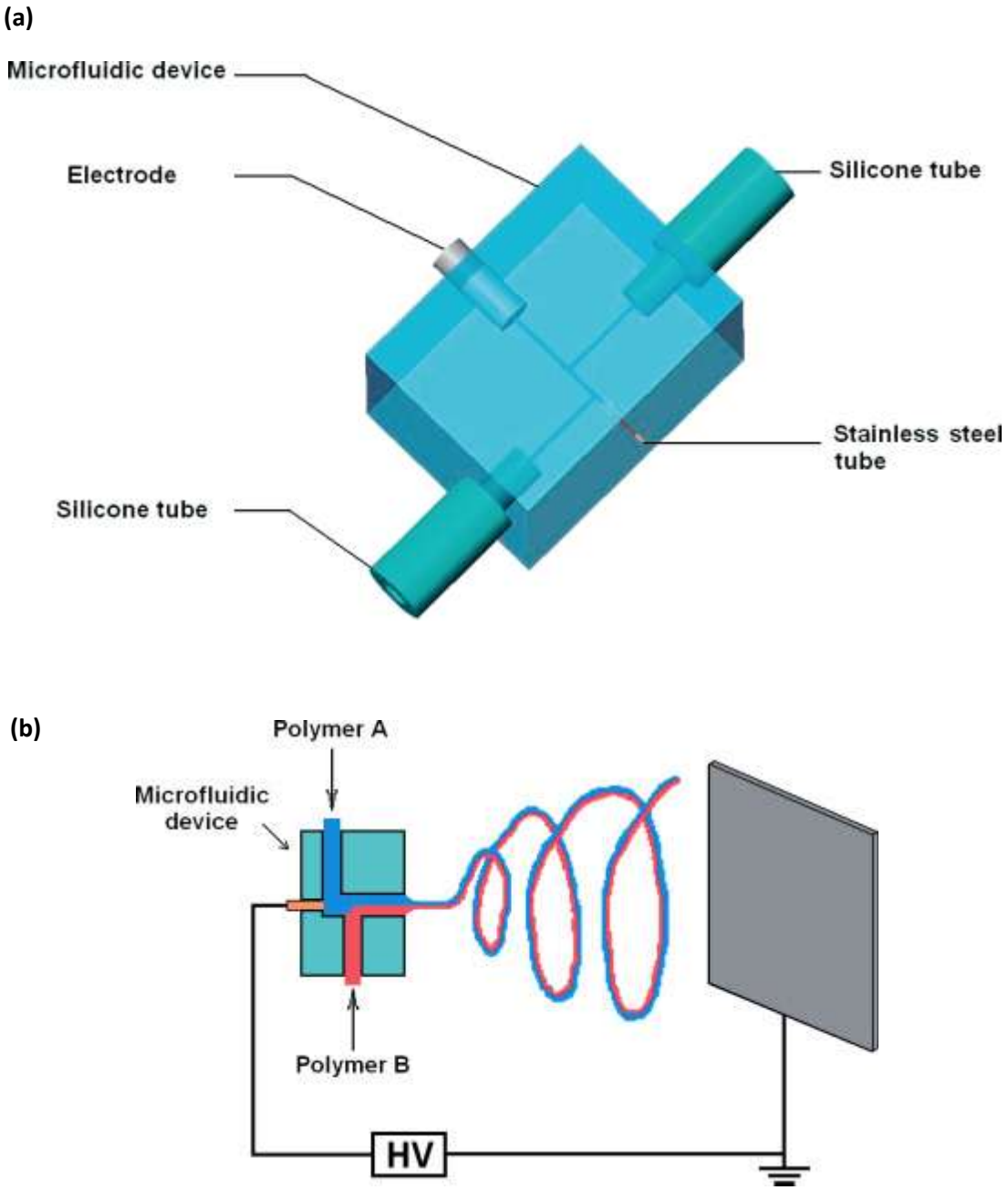

Figure 19. (a) The microfluidic device as the electrospinning spinneret. (b) Side-by-side electrospinning apparatus [32].

Lin's spinneret device is not necessarily better for the formation of SBS structure then the one used in the present study. Mixing the two components in the channel a long distance before

coming to the tip, the two polymer solutions might come to a random existence pattern rather than strictly staying side-by-side. Yet this idea of using silicone elastomer to cast spinneret can be borrowed to design a better SBS spinneret.

An ideal SBS spinneret is illustrated in Figure 20. The two component polymer solutions should go through different channels before they meet at the very end of the tip. The needle tip of the spinneret is one single tube, rather than two tubes which is used for simplification in this current study. The joint of the two channels should be smoothly connected to the tip. The whole spinneret should be reusable and cleaned easily, like immersing in HFP solution. Manufacture of this device is difficult especially for the joint part. This was why the current tied-needle spinneret was used for substitution. But further exploration should be done to improve the current spinneret.

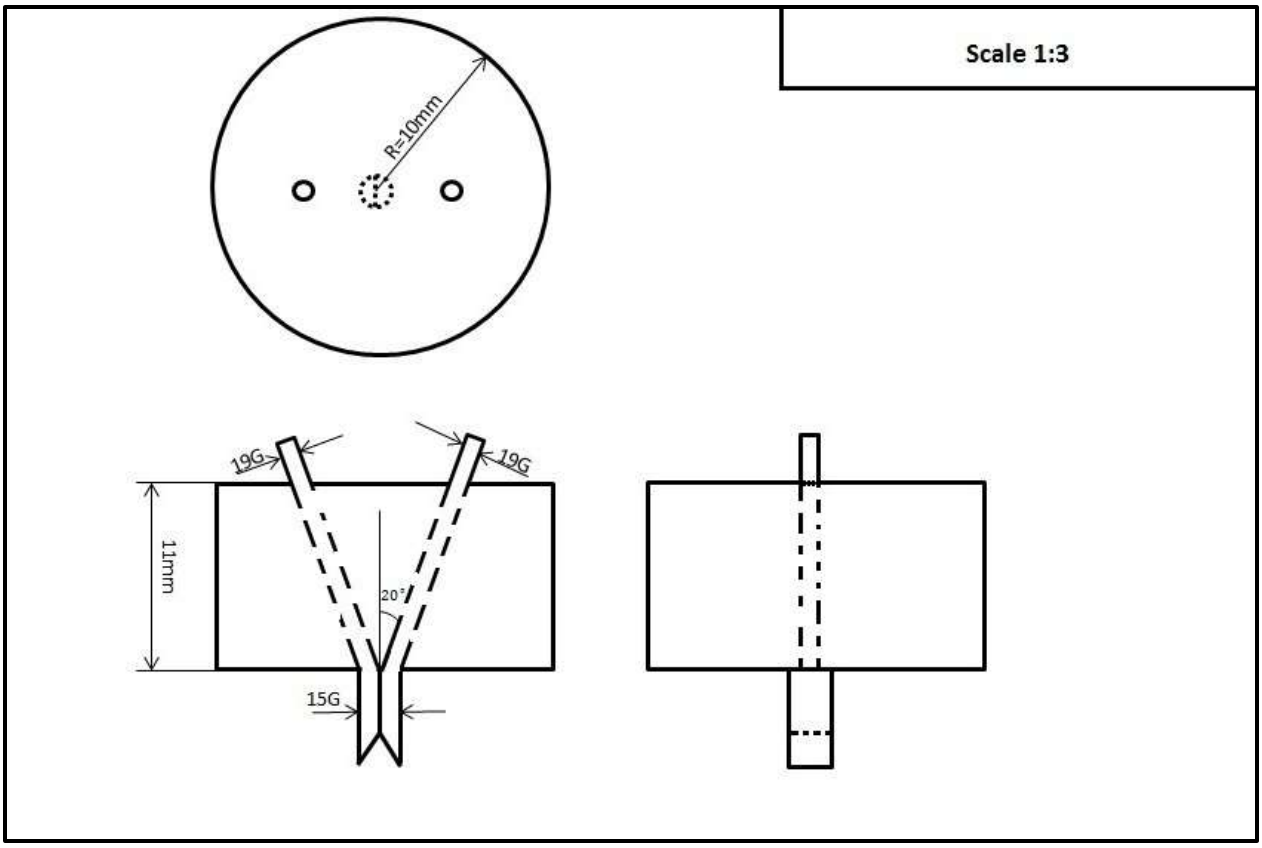

Figure 20. An ideal side-by-side bicomponent electrospinning spinneret design.

Self-crimp Formation of SBS Fibers

The formation of crimps in SBS fibers is crucial for this study. The polymer molecule chains are oriented during stretch, and then recoil during high temperature. The stretching temperature was chosen to be room temperature for the simplification of experiment. The heating temperature for recoil should be above T_g of one component, below T_g of the other component, and below the melting temperature of both components. According to the material properties of PLA and PCL used in this study, this heating temperature should be between -60~58 °C. The heating temperature should also be higher than stretching temperature (24 °C), and the higher,

the better in order to gain prominent crimps. A heating temperature of 55 °C and 50 °C was applied in the trials of this study, but the scaffolds, especially the non-SBS bicomponent scaffold shrank so severely that no enough area exists for sampling for the tests. A lower temperature, 48 °C was eventually chosen as comprise.

In a future study, the crimp formation mechanism of side-by-side fibers needs to be fully explored and different post treatment conditions can be tried to find the optimized one.

Scaffold Characterization

The SEM micrograph provided a powerful evidence for the SBS bicomponent structure. A further study can measure the fiber diameters and pore sizes of each scaffold, which can be used to explore the formation mechanism of crimps. Other than microscopy, chemical and physical characterization can also be done to identify the structure of the SBS scaffolds. For example, differential scanning calorimetry (DSC) can be used to evaluate the thermal characteristics of SBS scaffold.

The uniaxial tensile test indicated that the stretching and heat treatment to the SBS scaffolds didn't significantly affect most aspects of the scaffold's tensile properties. A larger number of samples can be pooled to evaluate tensile property differences caused by processing and/or the SBS structure. Additionally, other mechanical tests such as shear test and dynamic mechanical analysis can be performed to establish a more comprehensive understanding of the SBS bicomponent material.

Single fiber characterization is very difficult because of its extremely small scale. But analyzing a bundle of fibers, namely a filament, can help us better understand fiber properties.

Dalton et al. reported a way of electrospinning with dual collection rings to create a multi-filament yarn [40]. If side-by-side fibers are spun into this multi-filament yarn form, it would be very interesting to explore the filament properties. It might supplement the study of the scaffold as a whole.

Porosity test did not point to a significant improvement of crimped SBS fibers compared to unprocessed fibers. Yet the cell response test verified the hypothesis that crimped SBS fiber scaffold provides a better environment for cell ingrowth. Considering the electrospun scaffolds in all the four groups in this study have fairly high porosity, the value of porosity might become a less important factor in affecting cell growth, whereas the shape and interconnectivity of the pores are more dominant factors.

Conclusion

Though widely recognized in the textile industry, the formation mechanism of crimps of side-by-side bicomponent fibers are not fully utilized in the electrospinning applications. Unlike the previously published papers [32, 37, 41, 42], this study not only successfully created the side-by-side fiber structure by electrospinning, but also used room temperature stretching and high temperature treatment to generate significant crimps on the fibers.

Micrographs demonstrated the existence of side-by-side structured fibers and revealed the morphology differences between post-treated scaffolds and scaffolds directly collected from the mandrel. The quantitative porosity did not see a dramatic change as electrospun biomaterials typically have fairly high porosity (70 ~ 90% void fraction, [10]). However, the cell response test on crimped side-by-side scaffold showed improved cell ingrowth compared of non-crimped scaffolds. This also confirmed that it is not only the quantitative porosity that affects cell migration, but also the morphology of pores is crucial. Uniaxial tensile test discovered no significant changes between untreated side-by-side scaffolds and crimped side-by-side scaffolds. This result proved that the stretching and heating process did not bring about a harsh damage to the material. The sufficient mechanical strength would guarantee the potential application of side-by-side crimped fibers in tissue engineering.

The results of this study were quite inspiring. It introduced the concept of self-crimping side-by-side fibers into electrospinning, providing a new direction for biomaterials research. Further investigation on the crimping formation mechanism and optimization of crimping conditions can be done. The side-by-side electrospinning apparatus can be further specialized. For future studies, larger sample sizes and a more complete physical, chemical and biomedical characterization of this new material can be examined.

List of References

List of References

1. Organ Procurement and Transplantation Network (OPTN) and Scientific Registry of Transplant Recipients (SRTR). *OPTN / SRTR 2010 Annual Data Report*. Rockville, MD: Department of Health and Human Services, Health Resources and Services Administration, Healthcare Systems Bureau, Division of Transplantation; 2011: p. 12
2. J. Chlupac, E. Filova, and L. Bacakova, *Blood Vessel Replacement: 50 years of Development and Tissue Engineering Paradigms in Vascular Surgery*. Physiological Research, 2009. **58 (Suppl. 2):** p. 119-139.
3. Bernhard Ø. Palsson, and Sangeeta N. Bhatia, *Tissue Engineering*. 2004, Upper Sadle River, New Jersey: Pearson Prentice Hall. p. 20-33.
4. Ulrich A. Stock, and Joseph P. Vacanti, *Tissue Engineering: Current State and Prospects*. Annual Review of Medicine. 2001. **52**: p. 443-451
5. Langer, R., and Joseph P. Vacanti, *Tissue Engineering.* Science, 1993. **260**: p. 920-925.
6. I. Armentano, M. Dottori, E. Fortunati, S. Mattioli, and J.M. Kenny, *Biodegradable Polymer Matrix Nanocomposites for Tissue Engineering: A Review*. Polymer Degradation and Stability, 2010. **95**: p. 2126-2146.

7. Dietmar W. Hutmacher, *Scaffold Design and Fabrication Technologies for Engineering Tissues – State of the Art and Future Perspectives.* Journal of Biomaterials Science, Polymer Edition, 2001. **12**(1): p. 107-124.
8. David C. Brewster, *Current Controversies in the Management of Aortoiliac Occlusive Disease*. Journal of Vascular Surgery, 1997. **25**: p.365-379.
9. P. Klinkert, P.N. Post, P.J Breslau, and J.H van Bockel, *Saphenous Vein Versus PTFE for Above-Knee Femoropopliteal Bypass. A Review of the Literature*. European Journal of Vascular and Endovascular Surgery, 2004. **27**: p. 357-362.
10. Joseph Lowery, Silvia Panseri, Carla Cunha, and Fabrizio Gelain, *Elelctrospinning for Tissue Engineering Applications,* In: *Electrospinning Process and Nanofiber Research*, A.K. Haghi, and G.E. Zaikov, Editors. 2011, Nova Science Publishers, Inc.: New York. p. 127-149.
11. Catherine P. Barnes, Charles W. Pemble IV, David D. Brand, David Simpson, and Gary L. Bowlin, *Cross-Linking Electrospun Type II Collagen Tissue Engineering Scaffolds with Carbodiimide in Ethanol*. Tissue Engineering, 2007. **13**(7): p. 1593-1605.
12. John F. Cooley, et al., "Apparatus for Electrocally Dispersing Fluids." U.S. Patent No. 692631, issued Feb 4, 1902.
13. William James Morton, et al., "Method of Dispersing Fluids." U.S. Patent No. 705691, issued Jul. 29, 1902.
14. Geoffrey Taylor, *Disintegration of Water Drops in an Electric Field*. Proceedings of the Royal Society of London. Series A, Mathematical and Physical Sciences, 1964. **280**(1382): p. 383-397.

15. Geoffrey Taylor, *The Force Exerted by an Electric Field on a Long Cylindrical Conductor*. Proceedings of the Royal Society of London. Series A, Mathematical and Physical Sciences, 1966. **291**(1425): p. 145-158.
16. Geoffrey Taylor, *Electrically Driven Jets*. Proceedings of the Royal Society of London. Series A, Mathematical and Physical Sciences, 1969. **313**(1515): p.453-475.
17. J. Doshi, and D.H. Reneker, *Electrospinning Process and Applications of Electrospun Fibers*. Journal of Electrostatics, 1995. **35**: p.151-160.
18. F. Croisier, A.-S. Duwez, C.Jerome, A.F. Leonard, K.O. van der Werf, P.J. Dijkstra, and M.L. Bennink, *Mechanical Testing of Electrospun PCL fibers*. Acta Biomaterialia, 2012. **8**: p. 218-224.
19. Shanta Raj Bhattarai, Narayan Bhattarai, Ho Keun Yi, Pyong Han Hwang, Dong Il Cha, and Hak Yong Kim, *Novel Biodegradable Electrospun Membrane: Scaffold for Tissue Engineering*. Biomaterials, 2004. **25**: p. 2595-2602.
20. Avinash Baji, Yiu-Wing Mai, Shing-Chung Wong, Mojtaba Abtahi, and Pei Chen, *Electrospinning of Polymer Nanofibers: Effects on Oriented Morphology, Structures and Tensile Properties*. Composites Science and Technology, 2010. **70**: p. 703-718.
21. Yasmin Srivastava, Manuel Marquez, and Todd Thorsen, *Multijet Electrospinning of Conducting Nanofibers from Microfluidic Manifolds.* Journal of Applied Polymer Science, 2007. **106**: p. 3171-3178.
22. http://218.189.210.187/ApparelKey/Document/Cate2/2.4/wool_structure.htm
23. M. Horio, and T. Kondo, *Crimping of Wool Fibers*. Textile Research Journal, 1953. **23**: p. 373-386.

24. M. Horio, and T. Kondo, *Theory and Morphology of Crimped Rayon Staple*. Textile Research Journal, 1953. **23**: p. 137-151.

25. R.D.B. Fraser, H. Lindley and G.E. Rogers, *Chemical Heterogeneity and Cortical Segmentation in Wool*. Biochimica et biophysica acta, 1954. **13**(2): p.295-297.

26. R.D.B. Fraser, and G.E. Rogers, *The Origin of Segmentation in Wool Cortex.* Biochimica et biophysica acta, 1954. **13**(2): p.297-298.

27. "Bicomponent Fibers", http://web.utk.edu/~mse/Textiles/Bicomponent%20fibers.htm

28. Zhaoyang Liu, Darren Delai Sun, Peng Guo, and James O. Leckie, *An Efficient Bicomponent TiO_2/SnO_2 Nanofiber Photocatalyst Fabricated by Electrospinning with a Side-by-Side Dual Spinneret Method.* Nano Letters, 2007. **7**(4): p. 1081-1085.

29. Lizeth Adriana Garcia, Eduardo Arias, Ivana Moggio, Jorge Romero, Antonio Ledezma, Arturo Ponce, and Odilia Perez, *Fluorescent Core-Sheath Fibers by Electrospinning of a Phenyleneethynylene/Poly(styrene-co-maleimide) Blend*. Polymer, 2011. **52**: p. 5326-5334.

30. Dan Li, and Youman Xia, *Direct Fabrication of Composite and Ceramic Hollow Nanofibers by Electrospinning*. Nano Letters, 2004. **4**(5): p.933-938.

31. Pankaj Gupta, and Garth L. Wilkes, *Some Investigation on the Fibers Formation by Utilizing a Side-by-side Bicomponent Electrospinning Approach*. Polymer, 2003. **44**: 6353-6359.

32. Tong Lin, Hongxia Wang, and Xungai Wang, *Self-Crimping Bicomponent Nanofibers Electrospun from Polyacrylonitrile and Elastomeric Polyurethane*. Advanced Materials, 2005. **17**: p. 2699-2703.

33. Gina L. Fiore, Feng Jing, Victor G. Young, Jr., Christopher J. Cramer and Marc A. Hillmyer, *High T_g Aliphatic Polyesters by the Polymerization of Spirolactide Derivatives*. Polymer Chemistry, 2010. **1**(6): p. 870-877.

34. Shoufeng Yang, Kah-Fai Leong, Zhaohui Du, and Chee-Kai Chua, *The Design of Scaffolds for Use in Tissue Engineering: Part I. Traditional Factors*. Tissue Engineering, 2001. **7**(6): p. 679-689.

35. Nadia Ljungberg, and Bengt Wesslen, *The Effects of Plasticizers on the Dynamic Mechanical and Thermal Properties of Poly(Lactic Acid).* Journal of Applied Polymer Science, 2002. **86**(2): p. 1227–1234.

36. O. Martin, and L. Averous, Poly(lactic acid): *Plasticization and Properties of Biodegradable Multiphase Systems*. Polymer, 2001. **42**: p. 6209-6219.

37. Kyung-Ho Roh, David C. Martin, and Joerg Lahann, *Biphasic Janus Particles with Nanoscale Anisotropy*. Nature Materials, 2005. **4**(10), p. 759-763.

38. "Needle Gauge Comparison Chart", http://en.wikipedia.org/wiki/Needle_gauge_comparison_chart

39. Scott A. Sell, Michael P. Francis, Koyal Garg, Michael J. McClure, David G. Simpson and Gary L. Bowlin, *Cross-linking Methods of Electrospun Fibrinogen Scaffolds for Tissue Engineering Applications*. Biomedical Materials, 2008. **3**(4): p. 045001.

40. Paul D. Dalton, Doris Klee, and Martin Moller, *Electrospinning with Dual Collection Rings*. Polymer, 2005. **46**: p. 611-614.

41. Denver C. Surrao, James W.S. Hayami, Stephen D. Waldman, and Brian G. Amsden, *Self-Crimping, Biodegradable, Electrospun Polymer Microfibers.* Biomacromolecules, 2010. **11**: p. 3624-3629.

42. Lei Li, and You-Lo Hsieh, *Chitosan Bicomponent Nanofibers and Nanoporous Fibers. Carbohydrate Research*, 2006. **341**: p. 374-381.